AFRL-AFOSR-VA-TR-2021-0039

Theoretical/Computational Studies of High-Temperature Superconductivity from Quantum Magnetism

Rodriguez, Jose
CALIFORNIA STATE UNIVERSITY AUXILIARY SERVICES INC
230 W 41ST STREET FL 7
NEW YORK, NY, 90032-4226
US

05/27/2021
Final Technical Report

Air Force Research Laboratory
Air Force Office of Scientific Research
Arlington, Virginia 22203
Air Force Materiel Command

REPORT DOCUMENTATION PAGE

Form Approved
OMB No. 0704-0188

1. REPORT DATE *(DD-MM-YYYY)*	**2. REPORT TYPE**	**3. DATES COVERED** *(From - To)*
27-05-2021	Final	15 Jul 2017 - 14 Jan 2021

4. TITLE AND SUBTITLE
Theoretical/Computational Studies of High-Temperature Superconductivity from Quantum Magnetism

5a. CONTRACT NUMBER

5b. GRANT NUMBER
FA9550-17-1-0312

5c. PROGRAM ELEMENT NUMBER
61102F

6. AUTHOR(S)
Jose Rodriguez

5d. PROJECT NUMBER

5e. TASK NUMBER

5f. WORK UNIT NUMBER

7. PERFORMING ORGANIZATION NAME(S) AND ADDRESS(ES)
CALIFORNIA STATE UNIVERSITY AUXILIARY SERVICES INC
230 W 41ST STREET FL 7
NEW YORK, NY 90032-4226
US

8. PERFORMING ORGANIZATION REPORT NUMBER

9. SPONSORING/MONITORING AGENCY NAME(S) AND ADDRESS(ES)
AF Office of Scientific Research
875 N. Randolph St. Room 3112
Arlington, VA 22203

10. SPONSOR/MONITOR'S ACRONYM(S)
AFRL/AFOSR RTA1

11. SPONSOR/MONITOR'S REPORT NUMBER(S)
AFRL-AFOSR-VA-TR-2021-0039

12. DISTRIBUTION/AVAILABILITY STATEMENT
A Distribution Unlimited: PB Public Release

13. SUPPLEMENTARY NOTES

14. ABSTRACT
The PI has carried out theoretical and computational research on iron-selenide high-Tc superconductors. The PI has found a hidden spin density wave (hSDW) groundstate over the iron 3dxz/3dyz orbitals that shows the correct electron-type Fermi surface pockets at the corner of the folded Brillouin zone upon doping by electrons. The exchange of hidden spin fluctuations between two electrons results in an instability to S+- superconductivity at electron doping, with isotropic Cooper pairs that alternate in sign between visible electron Fermi surface pockets and faint hole Fermi surface pockets. This prediction resolves the puzzling observation of an S-wave energy gap by angle-resolved photoemission spectroscopy (ARPES) in iron-selenide superconductors.

15. SUBJECT TERMS

16. SECURITY CLASSIFICATION OF:			**17. LIMITATION OF ABSTRACT**	**18. NUMBER OF PAGES**	**19a. NAME OF RESPONSIBLE PERSON**
a. REPORT	**b. ABSTRACT**	**c. THIS PAGE**			KENNETH GORETTA
U	U	U	UU	17	**19b. TELEPHONE NUMBER** *(Include area code)* 426-7349

Final Report: (FA9550-17-1-0312) Theoretical/Computational Studies of High-Temperature Superconductivity from Quantum Magnetism*

Jose P. Rodriguez[1]

[1]*Department of Physics and Astronomy,*

California State University, Los Angeles, California 90032

Abstract

The PI has carried out theoretical and computational research on iron-selenide high-T_c superconductors. The PI has found a hidden spin density wave (hSDW) groundstate over the iron $3d_{xz}/3d_{yz}$ orbitals that shows the correct electron-type Fermi surface pockets at the corner of the folded Brillouin zone upon doping by electrons. The exchange of hidden spin fluctuations between two electrons results in an instability to S^{+-} superconductivity at electron doping, with isotropic Cooper pairs that alternate in sign between visible electron Fermi surface pockets and faint hole Fermi surface pockets. This prediction resolves the puzzling observation of an S-wave energy gap by angle-resolved photoemission spectroscopy (ARPES) in iron-selenide superconductors.

* Program Official: Dr. Kenneth C. Goretta, GHz-THz Electronics and Materials, Air Force Office of Scientific Research (AFOSR), Tel. (703) 696-7349, e-mail ghz.thz@us.af.mil.

The PI's previous-to-last funding cycle with the AFOSR ended in February 2016. His last funding cycle with the AFOSR began in July 2017, and it ended in January 2021. A summary of the work completed by the PI since March 2016 is given below. Specific publications that report on work funded by the AFOSR during this period are listed in bold numbers below. He received no other funding from the federal government during this period.

A. Quantum-Critical Spin-Density Waves versus Superconductivity in FeSe

The PI has studied the proposal that high-T_c iron-selenide superconductors lie near a quantum-critical point (QCP) that separates a true spin-density wave (SDW) of stripe or of checkerboard type from a *hidden* spin-density wave (hSDW) of checkerboard type. Figure 1 sketches the corresponding spin textures over the principal $3d_{xz}/3d_{yz}$ orbitals in iron superconductors. The quantum phase transition from the true SDW state to the hSDW

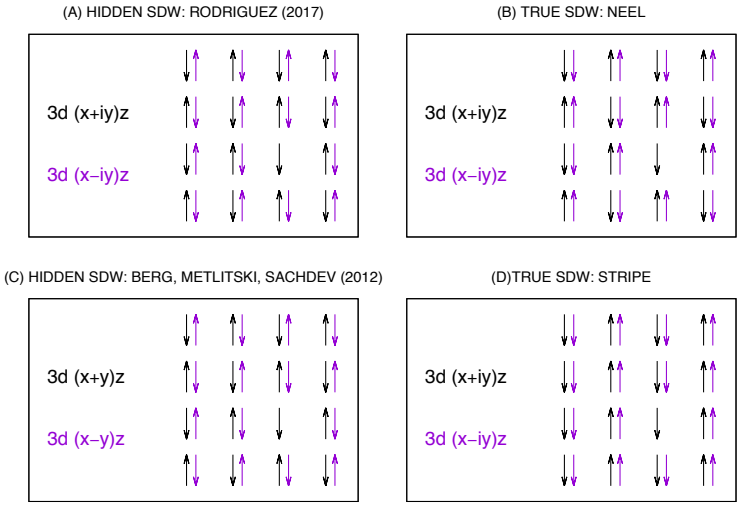

FIG. 1: Hidden spin-density waves, (a) ref. [1] and (c) ref. [2], versus true spin-density waves, (b) and (d). The former differ only in the orbitals. The missing spin represents a spin singlet in the case that one electron is added to half filling, while it simply represents a missing spin in the case that one electron is removed from half filling.

state is achieved by tuning down the strength of Hund's Rule. This effect is revealed by a local-moment model over the square lattice of iron atoms in a single layer of iron selenide

that has been introduced by the PI:

1. J.P. Rodriguez, "Isotropic Cooper Pairs with Emergent Sign Changes in a Single-Layer Iron Superconductor", *Physical Review B* **95**, 134511 (2017).

2. J.P. Rodriguez, "Particle-Hole Transformation in Strongly-Doped Iron-Based Superconductors", *Symmetry* **11**, 396 (2019).

The model Hamiltonian has the form

$$H_{tJ} = P(H_{\rm hop} + H_{\rm HH})P, \tag{1}$$

where $H_{\rm hop}$ represents hopping of an electron between the $d+ = (d_{xz} + id_{yz})/\sqrt{2}$ and the $d- = (d_{xz} - id_{yz})/\sqrt{2}$ orbitals across nearest neighbors of the square lattice of iron atoms, with matrix element $-t_1^{\perp}$. Also, at electron doping starting from half filling (one electron per site, per orbital), the operator P projects out states with unoccupied iron sites. Above, also, we have the Hund-Heisenberg Hamiltonian

$$\begin{aligned} H_{\rm HH} = & \sum_i J_0 \boldsymbol{S}_{i,d-} \cdot \boldsymbol{S}_{i,d+} + \sum_{\langle i,j\rangle} \sum_{\alpha} (J_1^{\parallel} \boldsymbol{S}_{i,\alpha} \cdot \boldsymbol{S}_{j,\alpha} + J_1^{\perp} \boldsymbol{S}_{i,\alpha} \cdot \boldsymbol{S}_{j,\bar{\alpha}}) \\ & + \sum_{\langle\langle i,j\rangle\rangle} J_2 (\boldsymbol{S}_{i,d+} + \boldsymbol{S}_{i,d-}) \cdot (\boldsymbol{S}_{j,d+} + \boldsymbol{S}_{j,d-}), \end{aligned} \tag{2}$$

where $\alpha = d-$ or $d+$. Here, J_0 is the Hund's Rule exchange coupling constant, which has a ferromagnetic (negative) sign, $J_1^{\parallel}$ and $J_1^{\perp}$ are the intra-orbital and inter-orbital Heisenberg exchange coupling constants across nearest neighbors, $\langle i,j\rangle$, and J_2 is the Heisenberg exchange coupling constant across next-nearest neighbors, $\langle\langle i,j\rangle\rangle$. The Heisenberg exchange coupling constants all have antiferromagnetic (positive) signs.

A Schwinger-boson-slave-fermion mean field theory analysis of the hSDW state (Fig. 1a) within the local moment model (1) yields a quantum-critical point that exists at moderate Hund's Rule coupling $-J_{0c}$, at which the spin-excitation spectrum collapses to zero energy at stripe SDW wave numbers $(\pi/a, 0)$ and $(0, \pi/a)$. Specifically, the QCP occurs at[1, 3]

$$-J_{0c} = 2(J_1^{\parallel} - J_1^{\perp}) + 2t_1^{\perp} x/(1-x)^2 s_0 - 4J_2,$$

where x denotes the concentration of electron doping from half filling. It is depicted by the dashed line in Fig. 2. The hSDW is therefore stable at Hund's Rule coupling $-J_0$ below $-J_{0c}$, which is positive for $J_1^{\parallel} > J_1^{\perp} + 2J_2$.

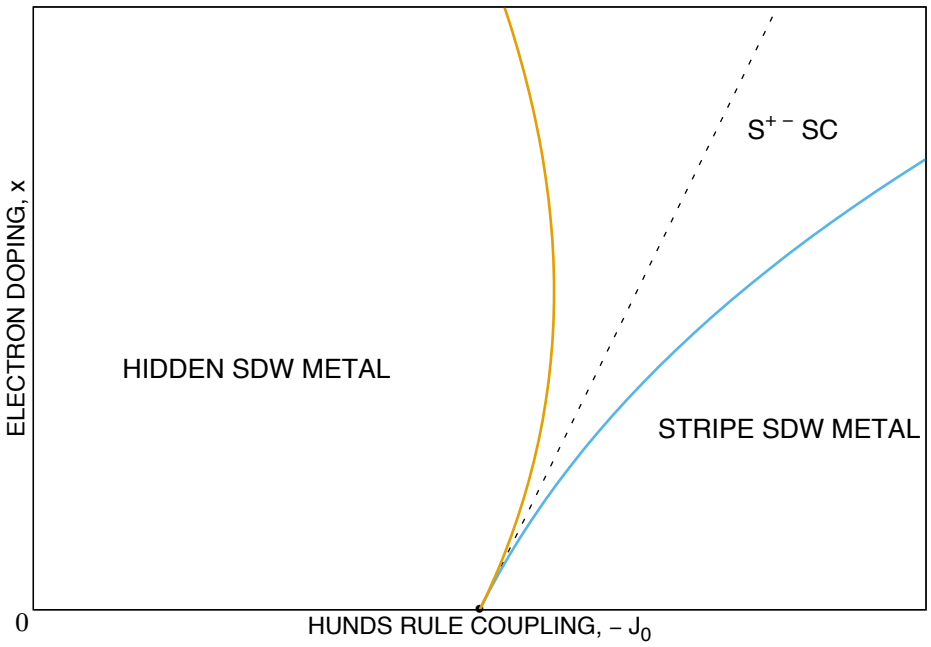

FIG. 2: Proposed phase diagram for local-moment model of electron-doped iron selenide (ref. [1]): Eqs. (1) and (2).

The PI and his graduate student Ronald Melendrez also introduced an extended Hubbard model over the square lattice of iron atoms in iron selenide that also exhibits the hSDW groundstate displayed by Fig. 1a:

3. J.P. Rodriguez and R. Melendrez, "Fermi Surface Pockets in Electron-Doped Iron Superconductor by Lifshitz Transition", *Journal of Physics Communications* **2**, 105011 (2018); "Corrigendum: Fermi Surface Pockets in Electron-Doped Iron Superconductor by Lifshitz Transition", *Journal of Physics Communications* **3**, 019501 (2019).

It coincides with the local-moment model (1) in the limit of strong on-site-orbital Coulomb repulsion. The Hamiltonian of the underlying extended Hubbard model[4] has three parts:

$$H_{\rm Hubbard} = H_{\rm hop} + H_U + H_{\rm sprx}. \tag{3}$$

On-site Coulomb repulsion is counted by the second term[**?**],

$$H_U = \sum_i \sum_\alpha U_0 n_{i,\alpha,\uparrow} n_{i,\alpha,\downarrow} + \sum_i J_0 \boldsymbol{S}_{i,d-} \cdot \boldsymbol{S}_{i,d+}. \tag{4}$$

where $n_{i,\alpha,s}$ is the occupation operator. Above, $U_0 > 0$ is the intra-orbital on-site Coulomb

repulsion energy. The third term in the Hamiltonian (3) represents super-exchange interactions among the iron spins via the selenium atoms:

$$H_{\rm sprx} = \sum_{\langle i,j\rangle} \; J_1^{(\rm sprx)}(\boldsymbol{S}_{i,d-} + \boldsymbol{S}_{i,d+}) \cdot (\boldsymbol{S}_{j,d-} + \boldsymbol{S}_{j,d+}) + \sum_{\langle\langle i,j\rangle\rangle} J_2^{(\rm sprx)}(\boldsymbol{S}_{i,d-} + \boldsymbol{S}_{i,d+}) \cdot (\boldsymbol{S}_{j,d-} + \boldsymbol{S}_{j,d+}). \tag{5}$$

Above, $J_1^{(\rm sprx)}$ and $J_2^{(\rm sprx)}$ are positive super-exchange coupling constants over nearest neighbor and next-nearest neighbor iron sites. Last, the electronic kinetic energy is governed by the hopping Hamiltonian $H_{\rm hop}$. It contains intra-orbital ($\|$) and inter-orbital ($\perp$) hopping across nearest neighbors of the square lattice of iron atoms, with real matrix elements $-t_1^{\|}$ and $-t_1^{\perp}$ that show s-wave and d-wave symmetry, respectively. It also contains inter-orbital hopping across next-nearest neighbors, with a pure imaginary matrix element $\mp t_2^{\perp}$ that shows d-wave symmetry[4].

For an electron of a given crystal momentum $\hbar\boldsymbol{k}$, the above hopping Hamiltonian $H_{\rm hop}$ then has intra-orbital and inter-orbital matrix elements

$$\varepsilon_{\|}(\boldsymbol{k}) = -2t_1^{\|}(\cos k_x a + \cos k_y a) \quad \text{and} \tag{6a}$$

$$\varepsilon_{\perp}(\boldsymbol{k}) = -2t_1^{\perp}(\cos k_x a - \cos k_y a) - 2t_2^{\perp}(\cos k_+ a - \cos k_- a), \tag{6b}$$

with $k_\pm = k_x \pm k_y$. It is easily diagonalized by plane waves in $d_{x(\delta)z}$ and $d_{y(\delta)z}$ orbitals that are rotated with respect to the principal axes by an angle $\delta(\boldsymbol{k})$:

$$\begin{aligned} |\boldsymbol{k}, d_{x(\delta)z}\rangle\rangle &= \mathcal{N}^{-1/2} \sum_i e^{i\boldsymbol{k}\cdot\boldsymbol{r}_i}[e^{i\delta(\boldsymbol{k})}|i,d+\rangle + e^{-i\delta(\boldsymbol{k})}|i,d-\rangle], \\ i|\boldsymbol{k}, d_{y(\delta)z}\rangle\rangle &= \mathcal{N}^{-1/2} \sum_i e^{i\boldsymbol{k}\cdot\boldsymbol{r}_i}[e^{i\delta(\boldsymbol{k})}|i,d+\rangle - e^{-i\delta(\boldsymbol{k})}|i,d-\rangle], \end{aligned} \tag{7}$$

where $\mathcal{N} = 2N_{\rm Fe}$ is the number of iron site-orbitals. The phase shift $\delta(\boldsymbol{k})$ is set by $\varepsilon_\perp(\boldsymbol{k}) = |\varepsilon_\perp(\boldsymbol{k})|e^{i2\delta(\boldsymbol{k})}$. The energy eigenvalues of the bonding (+) and anti-bonding (−) plane waves (7) are respectively given by $\varepsilon_+(\boldsymbol{k}) = \varepsilon_\|(\boldsymbol{k}) + |\varepsilon_\perp(\boldsymbol{k})|$ and $\varepsilon_-(\boldsymbol{k}) = \varepsilon_\|(\boldsymbol{k}) - |\varepsilon_\perp(\boldsymbol{k})|$.

Notice that the above energy bands satisfy the perfect nesting condition

$$\varepsilon_\pm(\boldsymbol{k} + \boldsymbol{Q}_{\rm AF}) = -\varepsilon_\mp(\boldsymbol{k}), \tag{8}$$

where $\boldsymbol{Q}_{\rm AF} = (\pi/a, \pi/a)$ is the wavevector for the checkerboard on the square lattice of iron atoms. The Fermi level at half filling therefore lies at $\epsilon_{\rm F} = 0$. Figure 3 shows such

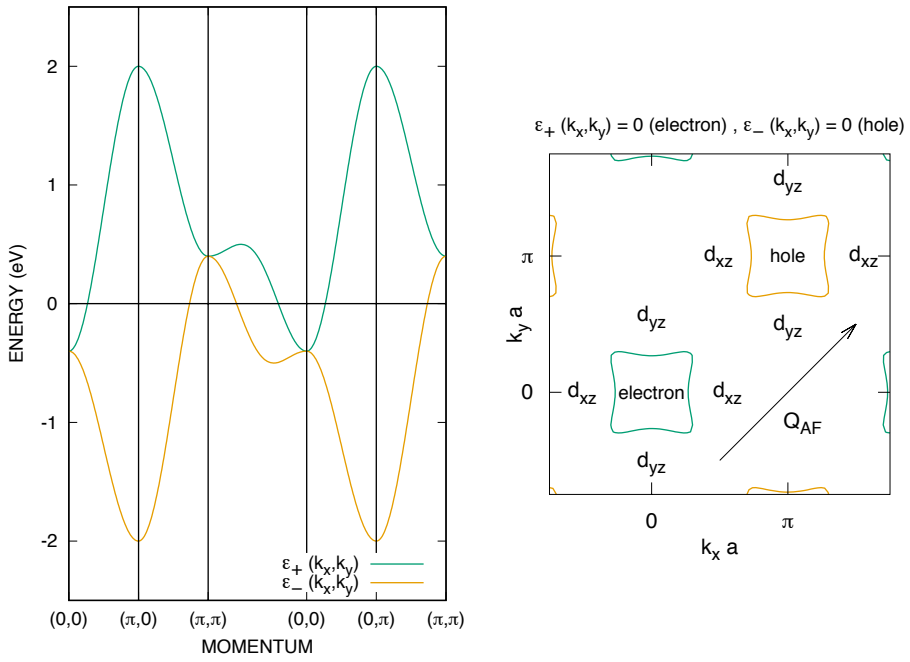

FIG. 3: Band structure with perfectly nested Fermi surfaces at half filling: $\varepsilon_+(\boldsymbol{k}) = 0$ and $\varepsilon_-(\boldsymbol{k}) = 0$, with hopping matrix elements $t_1^{\parallel} = 100$ meV, $t_1^{\perp} = 500$ meV, $t_2^{\parallel} = 0$, and $t_2^{\perp} = 100\,i$ meV.

perfectly nested electron-type and hole-type Fermi surfaces for hopping parameters $t_1^{\parallel} = 100$ meV, $t_1^{\perp} = 500$ meV, $t_2^{\parallel} = 0$ and $t_2^{\perp} = 100\,i$ meV. A mean field theory approximation of the extended Hubbard model (3) finds that the perfect nesting (8) results in an hSDW groundstate with a spin texture following Fig. 1a at strong enough magnetic frustration[4], $J_2^{(\mathrm{sprx})} > 0.5 J_1^{(\mathrm{sprx})}$.

B. Spin-Fermion Model, Fermi Surfaces, and Superconductivity in FeSe

The PI has shown in publication 3 above and in preprint 4 below that both the local-moment model (1) and the extended Hubbard model (3) reduce to a spin-fermion model, where the electrons in energy bands displayed by Fig. 3 interact with low-energy spin-wave excitations about the hSDW state shown by Fig. 1a:

4. J.P. Rodriguez, "Superconductivity by Hidden Spin Fluctuations in Electron-Doped Iron Selenide", submitted to *Physical Review B*, arXiv:2001.07908 .

The spin-fermion model has the form

$$H_{\rm spin-fermion} = H_{\rm hop} + H_{\rm e-hsw} + H_{\rm hsw}, \tag{9}$$

where $H_{\rm hop}$ is the previous electron hopping Hamiltonian, where $H_{\rm hsw}$ is the Hamiltonian for hidden spinwaves, and where $H_{\rm e-hsw}$ is the interaction Hamiltonian between the two. A mean field theory approximation of the extended Hubbard model (3) implies an isotropic interaction between hidden spinwaves and electrons of the form[4]

$$H_{\rm e-hsw} = -\sum_i \sum_\alpha U(\pi) \boldsymbol{m}_{i,\alpha} \cdot 2\boldsymbol{S}_{i,\alpha}, \quad \text{with} \quad U(\pi) = U_0 + \frac{1}{2} J_0. \tag{10}$$

Above, $\boldsymbol{m}_{i,\alpha}$ denotes the magnetic moment due to spin fluctuations about the hSDW state, at iron site i, in orbital α. The *true* magnetic moment per iron site is defined by $\boldsymbol{m}_i(0) = \boldsymbol{m}_{i,d+} + \boldsymbol{m}_{i,d-}$, while the *hidden* magnetic moment per iron site is defined by $\boldsymbol{m}_i(\pi) = \boldsymbol{m}_{i,d+} - \boldsymbol{m}_{i,d-}$. The Hamiltonian above that describes hidden spin fluctuations, $H_{\rm hsw}$, is then a functional of the conjugate variables $\boldsymbol{m}_i(0)$ and $\boldsymbol{m}_i(\pi)$. It describes the well-known antiferromagnetic resonance identified first by Phillip Anderson[5–7], specifically for low-energy hidden spinwaves. The propagator for hidden spinwaves is given by $\langle m^{(a)}(\pi) m^{(b)}(\pi) \rangle|_{\boldsymbol{q},\omega} = \delta_{a,b} i D(\boldsymbol{q},\omega)$ for $a, b = x, y$, or z, where

$$D(\boldsymbol{q},\omega) = \frac{(2s_1)^2}{\chi_\perp} [\omega^2 - \omega_b^2(\boldsymbol{q})]^{-1} \tag{11}$$

at long wavelength and low frequency[6, 7]. Here, $2s_1\hbar$ is the magnitude of the hidden ordered magnetic moment, $\boldsymbol{m}(\pi)$, at an iron site, while $\chi_\perp$ denotes the transverse spin susceptibility of the hSDW state. Above, the poles in frequency coincide with the spectrum for hidden spinwaves. They disperse from zero energy at the checkerboard wavevector $\boldsymbol{Q}_{\rm AF} = (\pi/a, \pi/a)$ as

$$\omega_b(\boldsymbol{q}) = \sqrt{c_b^2 |\bar{\boldsymbol{q}}|^2 + \Delta_b^2}, \tag{12}$$

where $\bar{\boldsymbol{q}} = \boldsymbol{q} + \boldsymbol{Q}_{\rm AF}$. The velocity of the hidden spinwaves is denoted by c_b, while the spin gap Δ_b is null when the hSDW state shows long-range order.

The PI has exploited the spin-fermion model (9)-(12) above to obtain the electron Fermi surface pockets at the corner of the folded Brillouin zone that are characteristic of electron-doped iron selenide starting from the original Fermi surfaces shown in Fig. 3. To do this, he first derived an Eliashberg Theory[8, 9] for the wave function renormalizations, $Z_n(\boldsymbol{k},\omega)$, for

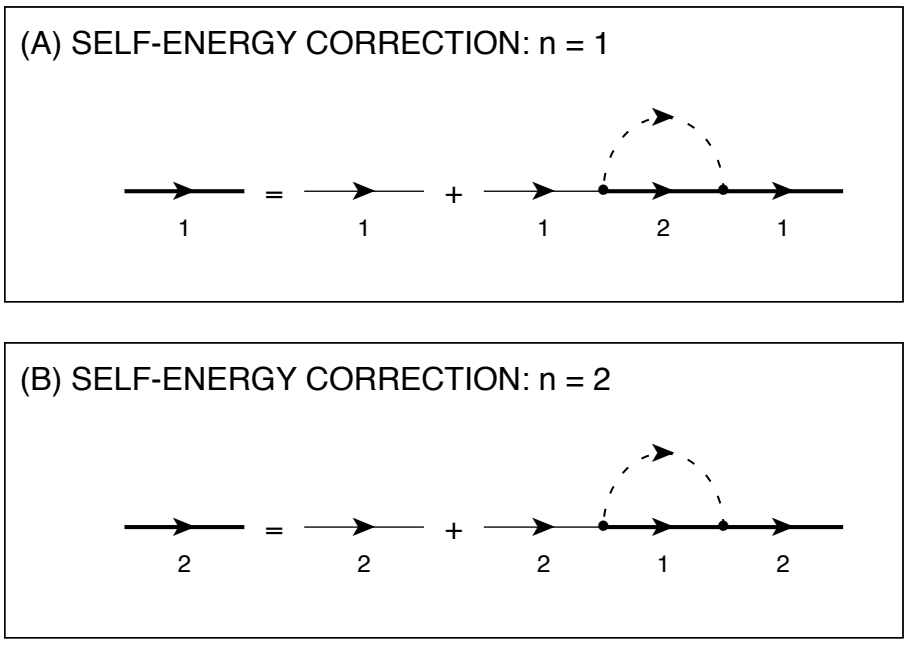

FIG. 4: Feynman diagrams for electron propagator with purely inter-band scattering, in the absence of vertex corrections.

the shifts of the energy bands, $\mu_n(\boldsymbol{k}, \omega)$, and for the superconducting energy gaps, $\Delta_n(\boldsymbol{k}, \omega)$, following the self-consistent approximation depicted by Fig. 4. Here, $n = 1$ and $n = 2$ denote the anti-bonding $(-)$ band and the bonding $(+)$ band, respectively, while $1/Z_n$ is the residue (amplitude) of the electronic pole in frequency (quasi-particle energy). A standard Nambu-Gorkov Greens function approach[10–13] yields the following Eliashberg equations

for these three quantities at zero temperature[14]:

$$
\begin{aligned}
[Z_n(\boldsymbol{k},\omega)-1]\omega \;&=\; \frac{3}{2}\int \frac{d^2k'}{(2\pi)^2}U^2(\pi)\frac{s_1^2}{\chi_\perp}\frac{\sin^2[\delta(\boldsymbol{k})+\delta(\boldsymbol{k}')]}{Z_{\bar{n}}(\bar{\boldsymbol{k}}',\omega')}\cdot \\
&\quad\cdot\frac{1}{2\omega_b(\boldsymbol{q})}\left[\frac{1}{\omega_b(\boldsymbol{q})+E_{\bar{n}}(\bar{\boldsymbol{k}}')-\omega}-\frac{1}{\omega_b(\boldsymbol{q})+E_{\bar{n}}(\bar{\boldsymbol{k}}')+\omega}\right], \\
\mu_0-\mu_n \;&=\; -\frac{3}{2}\int \frac{d^2k'}{(2\pi)^2}U^2(\pi)\frac{s_1^2}{\chi_\perp}\frac{\sin^2[\delta(\boldsymbol{k})+\delta(\boldsymbol{k}')]}{Z_{\bar{n}}(\bar{\boldsymbol{k}}',\omega')}\frac{\varepsilon_{\bar{n}}(\bar{\boldsymbol{k}}')-\mu_{\bar{n}}}{Z_{\bar{n}}(\bar{\boldsymbol{k}}',\omega')E_{\bar{n}}(\bar{\boldsymbol{k}}')}\cdot \\
&\quad\cdot\frac{1}{2\omega_b(\boldsymbol{q})}\left[\frac{1}{\omega_b(\boldsymbol{q})+E_{\bar{n}}(\bar{\boldsymbol{k}}')-\omega}+\frac{1}{\omega_b(\boldsymbol{q})+E_{\bar{n}}(\bar{\boldsymbol{k}}')+\omega}\right], \\
Z_n(\boldsymbol{k},\omega)\Delta_n(\boldsymbol{k},\omega) \;&=\; -\frac{3}{2}\int \frac{d^2k'}{(2\pi)^2}U^2(\pi)\frac{s_1^2}{\chi_\perp}\frac{\sin^2[\delta(\boldsymbol{k})+\delta(\boldsymbol{k}')]}{Z_{\bar{n}}(\bar{\boldsymbol{k}}',\omega')}\frac{\Delta_{\bar{n}}(\bar{\boldsymbol{k}}',\omega')}{E_{\bar{n}}(\bar{\boldsymbol{k}}')}\cdot \\
&\quad\cdot\frac{1}{2\omega_b(\boldsymbol{q})}\left[\frac{1}{\omega_b(\boldsymbol{q})+E_{\bar{n}}(\bar{\boldsymbol{k}}')-\omega}+\frac{1}{\omega_b(\boldsymbol{q})+E_{\bar{n}}(\bar{\boldsymbol{k}}')+\omega}\right],
\end{aligned}
\tag{13}
$$

with the excitation energy

$$
E_n(\boldsymbol{k},\omega)=\sqrt{\left[\frac{\varepsilon_n(\boldsymbol{k})-\mu_n}{Z_n(\boldsymbol{k},\omega)}\right]^2+\Delta_n^2(\boldsymbol{k})}. \tag{14}
$$

Above[11], $\omega'=E_{\bar{n}}(\bar{\boldsymbol{k}}')$, while $\bar{\boldsymbol{k}}=\boldsymbol{k}+\boldsymbol{Q}_{\rm AF}$. Also, μ_0 denotes the chemical potential.

At half filling, which corresponds to one electron per iron site, per orbital, and at strong Hubbard repulsion U_0, an analysis of the Eliashberg equations (13) in the critical normal state, $\Delta_n=0$ and $\Delta_b\to 0$, reveals a Lifshitz transition from the Fermi surfaces depicted by Fig. 3 to electron/hole pockets at the corner of the folded Brillouin zone depicted by Fig. 5. The Eliashberg equations therefore predict a hSDW at half filling due to nested Fermi surface pockets at the corner of the folded Brillouin zone. It must be emphasized, however, that the spectral weight of the renormalized Fermi surface pockets is vanishingly small at criticality[14]: $Z^{-1}\to 0$ as $\Delta_b\to 0$. This implies that the hSDW state at half filling is in fact a Mott insulator. It is also important to mention that these results for the Lifshitz transition confirm previous ones that start from the other side of the QCP at $\Delta_b=0$. They were based on an Eliashberg theory in the particle-hole channel for the long-range ordered hSDW state[4].

The PI also computed the corrections to the Lifshitz transition described above due to weak electron doping compared to half filling. In particular, he computed the variations

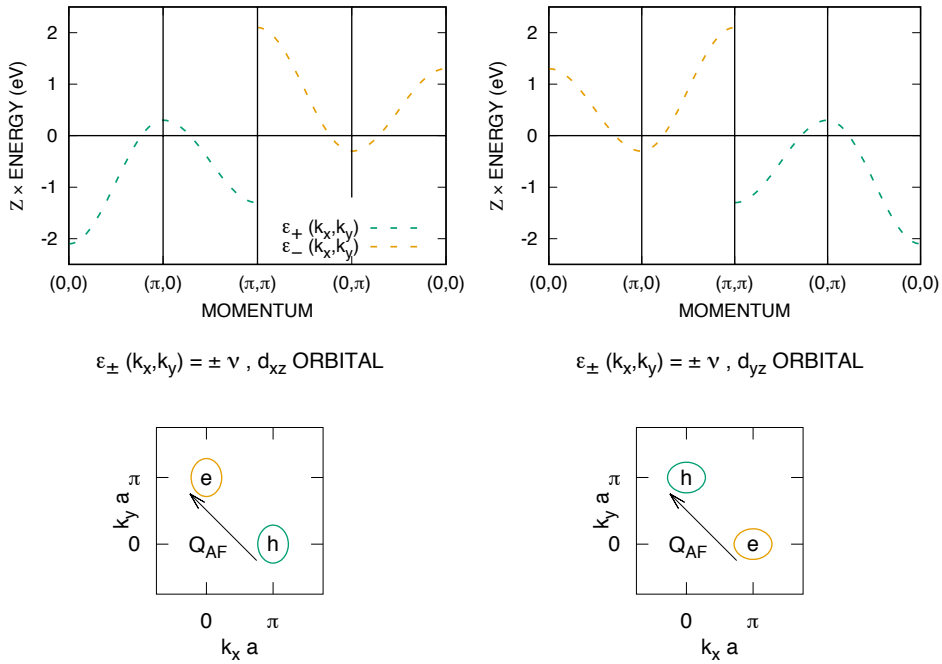

FIG. 5: Renormalized electron bands and Fermi surfaces at half filling after the Lifshitz transition. The orbital character is only approximate, although it becomes exact as the area of the Fermi surface pockets vanishes as U_0 diverges.

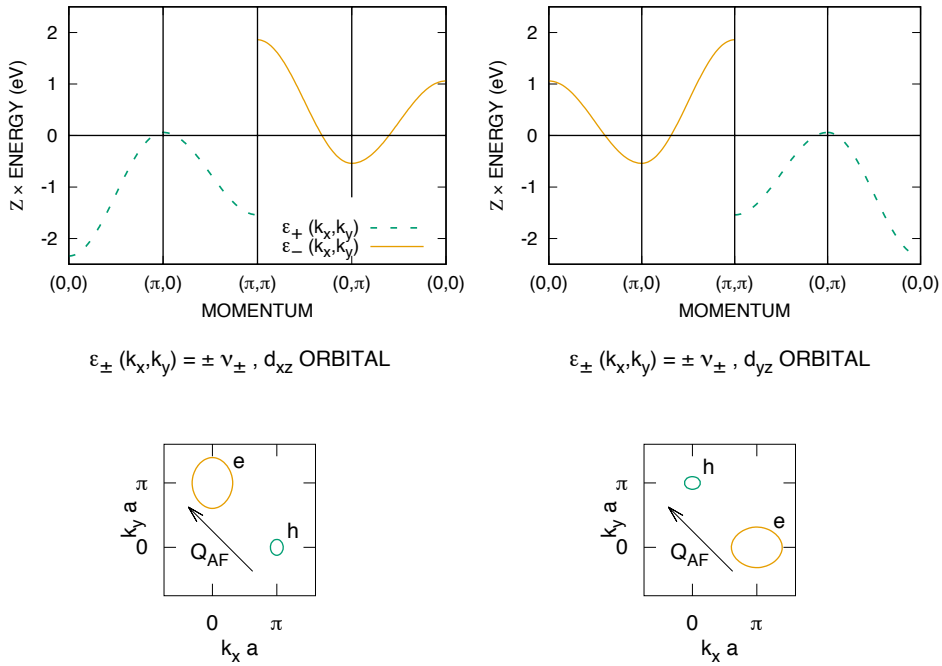

FIG. 6: Renormalized electron bands and Fermi surfaces at electron doping after the Lifshitz transition. Again, the orbital character is only approximate.

in the wave function renormalization, δZ_1 and δZ_2, and the variations in the shifts in the energy bands, $\delta\mu_1$ and $\delta\mu_2$, within linear response in the chemical potential, μ_0. Figure 6 summarizes the results of the linear-response calculation. First, it describes a *rigid* shift of both renormalized electron and hole bands shown in Fig. 5 upon injecting electrons into the system. As depicted by Fig. 6, the hole Fermi surface pockets thereby shrink, and the electron Fermi surface pockets thereby get bigger. Second, linear response in the chemical potential implies equal and opposite variations in the wavefunction renormalization, δZ_1 and δZ_2, proportional to $Z\mu_0$. In particular, the wave function renormalization increases for the hole bands, while it decreases for the electron bands. The solid lines versus the dashed lines in the renormalized bandstructure shown by Fig. 6 depict this result.

Last, the PI showed that the Eliashberg equations (13) harbor a Cooper pairing instability on the above electron Fermi surface pockets and faint hole Fermi surface pockets at the corner of the folded Brillouin zone. The Cooper pairs show S^{+-} symmetry, with a sign that alternates between the visible electron pockets and the faint hole pockets. This effect potentially accounts for the puzzling observation by ARPES of an isotropic energy gap over the electron Fermi surface pockets in high-temperature iron-selenide superconductors[15–23].

C. Spin Resonances and Quark Physics in Iron-Selenide Superconductors

Recent inelastic neutron scattering spectroscopy on organic-molecule intercalated iron selenides, which are also high-temperature superconductors, find spin excitations at energies above the superconducting gap[24] of 28 meV. Such above-gap spin excitations form a diamond in momentum space about the checkerboard wave vector $\boldsymbol{Q}_{\rm AF} = (\pi/a, \pi/a)$. (See Fig. 8.) The PI has recently shown that the hSDW state mentioned above predicts such "hollowed-out" spin excitations at momenta around $\boldsymbol{Q}_{\rm AF}$:

5. J.P. Rodriguez, "Spin Resonances in Iron-Selenide High-T_c Superconductors by Proximity to Hidden Spin Density Wave", *Physical Review B* **102**, 024521 (2020).

In particular, he calculated the dynamical spin susceptibility of the hSDW state within the random phase approximation (RPA), and he found a "floating ring" of spin excitations above a threshold energy, at momentum $\boldsymbol{Q}_{\rm AF}$ [25]. Figure 7 shows the beginnings of the threshold in energy. Figure 9 shows that the spin excitations form a diamond shape in

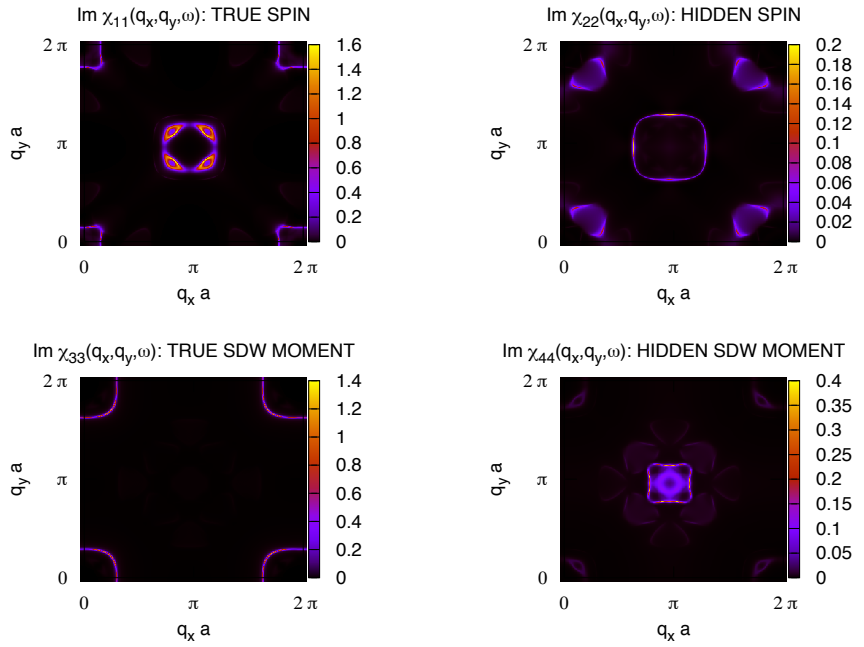

FIG. 7: Spin excitations at frequency $\omega = 350$ meV and damping rate $\Gamma = 16$ meV predicted by RPA over a periodic lattice of 300×300 iron atoms. Hopping parameters are listed in the caption to Fig. 3, while Hund and spin-exchange couplings are set to $J_0 = -100$ meV, $J_1 = 100$ meV, and $J_2 = 50$ meV. The Hubbard on-site repulsion is set to $U_0 = 7.37$ eV. (Rodriguez, Phys. Rev. B **102**, 024521 (2020), ref. [25].)

momentum space at energies above the threshold. Such spin resonances likely persist at energies above the quasi-particle gap in the S^{+-} Cooper pair state mentioned previously, which lies nearby the hSDW state in the phase diagram. (See Fig. 2.) The hSDW shown by Fig. 1a is therefore a promising parent groundstate for high-temperature iron-selenide superconductors.

The PI has also computed the renormalization of the interaction vertex (10) between electrons and hidden spinwaves. He has found that it displays a phenomenon shown by quarks, which are subatomic particles, called *asymptotic freedom* [26].

6. J.P. Rodriguez, "Quantum-Critical Spin-Density Waves in Iron-Selenide High-T_c Superconductors", submitted to *Frontiers in Physics*, arXiv:2006.05680 .

In particular, interactions between electrons and hidden spinwaves become weaker and weaker as the size of the system becomes bigger and bigger. The PI also argues that

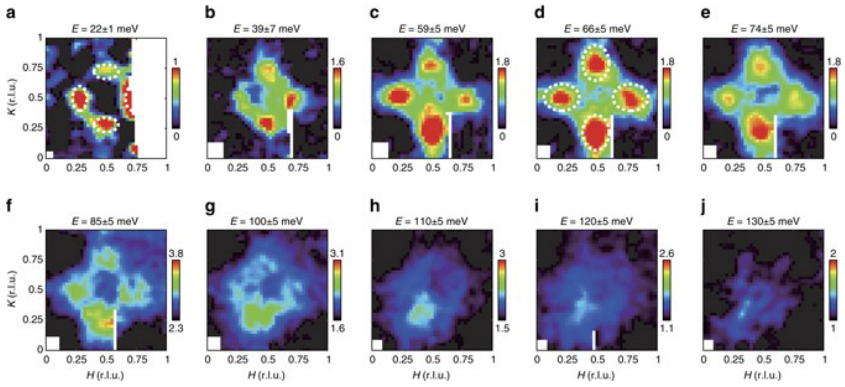

FIG. 8: Spin excitations in momentum space at constant energy in organic-molecule intercalated FeSe. (Pan et al., Nat. Commun. **8**,123 (2017), ref. [24].)

particle-hole excitations are confined together by "string-states" of overturned spins between the electron and the hole. The PI finally suggests that such quark-like physics leads to the confinement of hole excitations at the corner of the folded Brillouin zone depicted by Fig. 6.

D. Chromium Analogs to Iron-Pnictide Superconductors

The PI collaborated with Radi Jishi from his home institution and with AFRL scientists Tim Haugan and Mike Susner in a search for superconductivity in chromium pnictides.

7. R.A. Jishi, J.P. Rodriguez, T.J. Haugan and M.A. Susner, "Prediction of Antiferromagnetism in Barium Chromium Phosphide Confirmed after Synthesis", *Journal of Physics Condensed Matter* **32**, 025502 (2020).

In particular, powder samples of the compound $BaCr_2P_2$ were successfully grown at AFRL by Mike Susner and Tim Haugan. Density functional theory (DFT) calculations were performed

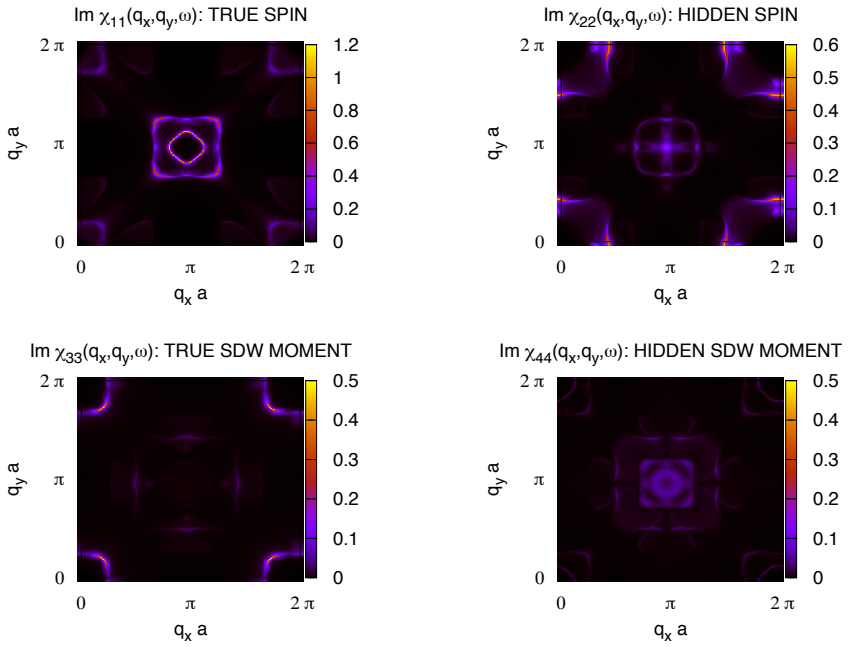

FIG. 9: Spin excitations at frequency $\omega = 500$ meV and damping rate $\Gamma = 16$ meV predicted by RPA over a periodic lattice of 300×300 iron atoms. Hopping parameters, Hund and spin-exchange couplings, and the Hubbard U_0 are identical to those used in Fig. 7. (Rodriguez, Phys. Rev. B **102**, 024521 (2020), ref. [25].)

by Radi Jishi at California State University Los Angeles, where the crystal structure was predicted to be of the $ThCr_2Si_2$ type, in common with the iron-pnictide parent compound $BaFe_2As_2$. The DFT prediction for the crystal structure was confirmed experimentally at AFRL by the collaborators there. A Néel antiferromagnetic groundstate over the chromium atoms was also predicted by DFT. The PI proposed that such antiferromagnetic order is due to nesting of the Fermi surfaces that is obscured by a Lifshitz transition in the topology of the Fermi surfaces.

[1] J.P. Rodriguez, "Isotropic Cooper Pairs with Emergent Sign Changes in a Single-Layer Iron Superconductor", Phys. Rev. B **95**, 134511 (2017).

[2] E. Berg, M.A. Metlitski and S. Sachdev, "Sign-Problem-Free Quantum Monte Carlo of the Onset of Antiferromagnetism in Metals", Science **338**, 1606 (2012).

[3] J.P. Rodriguez, "Magnetic Excitations in Ferropnictide Materials Controlled by a Quantum Critical Point into Hidden Order", Phys. Rev. B **82**, 014505 (2010).

[4] J.P. Rodriguez and R. Melendrez, "Fermi Surface Pockets in Electron-Doped Iron Superconductor by Lifshitz Transition", *J. Phys. Commun.* **2**, 105011 (2018); "Corrigendum: Fermi Surface Pockets in Electron-Doped Iron Superconductor by Lifshitz Transition", *J. Phys. Commun.* **3**, 019501 (2019).

[5] P.W. Anderson, "An Approximate Quantum Theory of the Antiferromagnetic Ground State", Phys. Rev. **86**, 694 (1952).

[6] B.I. Halperin and P.C. Hohenberg, "Hydrodynamic Theory of Spin Waves", Phys. Rev. **188**, 898 (1969).

[7] D. Forster, *Hydrodynamic Fluctuations, Broken Symmetry, and Correlation Functions* (Benjamin/Cummings), Reading, MA, 1975).

[8] G.M. Eliashberg, "Interactions between Electrons and Lattice Vibrations in a Superconductor", Sov. Phys. JETP **11**, 696 (1960).

[9] G.M. Eliashberg, "Temperature Green's Function for Electrons in a Superconductor", Sov. Phys. JETP **12**, 1000 (1961).

[10] J.R. Schrieffer, *Theory of Superconductivity* (Benjamin, New York, 1964).

[11] D.J. Scalapino, in *Superconductivity*, v. 1, ed. R.D. Parks (Dekker, New York, 1969).

[12] Y. Nambu, "Quasi-Particles and Gauge Invariance in the Theory of Superconductivity", Phys. Rev. **117**, 648 (1960).

[13] L.P. Gorkov, Zh. Eksperim. i Teor. Fiz. **34**, 735 1958; "About the Energy Spectrum of Superconductors", Sov. Phys. JETP **7**, 505 (1958).

[14] J.P. Rodriguez, "Superconductivity by Hidden Spin Fluctuations in Electron-Doped Iron Selenide", submitted to Physical Review B, arXiv:2001.07908 .

[15] M. Xu, Q. Q. Ge, R. Peng, Z. R. Ye, Juan Jiang, F. Chen, X. P. Shen, B. P. Xie, Y. Zhang, A.

F. Wang, X. F. Wang, X. H. Chen, and D. L. Feng, "Evidence for an S-Wave Superconducting Gap in $K_xFe_{2y}Se_2$ from Angle-Resolved Photoemission", Phys. Rev. B **85**, 220504(R) (2012).

[16] Q.-Y. Wang, Z. Li, W.-H. Zhang, Z.-C. Zhang, J.-S. Zhang, W. Li, H. Ding, Y.-B. Ou, P. Deng, K. Chang, J. Wen, C.-L. Song, K. He, J.-F. Jia, S.-H. Ji, Y. Wang, L. Wang, X. Chen, X. Ma, Q.-K. Xue, "Interface-Induced High-Temperature Superconductivity in Single Unit-Cell FeSe Films on $SrTiO_3$", Chin. Phys. Lett. **29**, 037402 (2012).

[17] D. Liu, W. Zhang, D. Mou, J. He, Y.-B. Ou,Q.-Y. Wang, Z. Li, L. Wang, L. Zhao, S. He, Y. Peng, X. Liu, C. Chaoyu, L. Yu, G. Liu, X. Dong, J. Zhang, C. Chen, Z. Xu, J. Hu, X. Chen, Z. Ma, Q. Xue and X.J. Zhou, "Electronic Origin of High-Temperature Superconductivity in Single-Layer FeSe Superconductor", Nat. Commun. **3**, 931 (2012).

[18] R. Peng, X.P. Shen, X. Xie, H.C. Xu, S.Y. Tan, M. Xia, T. Zhang, H.Y. Cao, X.G. Gong, J.P. Hu, B.P. Xie, D. L. Feng, "Measurement of an Enhanced Superconducting Phase and a Pronounced Anisotropy of the Energy Gap of a Strained FeSe Single Layer in FeSe/Nb: $SrTiO_3/KTaO_3$ Heterostructures Using Photoemission Spectroscopy", Phys. Rev. Lett. **112**, 107001 (2014).

[19] J.J. Lee, F.T. Schmitt, R.G. Moore, S. Johnston, Y.-T. Cui, W. Li, M. Yi, Z.K. Liu, M. Hashimoto, Y. Zhang, D.H. Lu, T.P. Devereaux, D.-H. Lee and Z.-X. Shen, "Interfacial Mode Coupling as the Origin of the Enhancement of T_c in FeSe Films on $SrTiO_3$", Nature **515**, 245 (2014).

[20] Q. Fan, W.H. Zhang, X. Liu, Y.J. Yan, M.Q. Ren, R. Peng, H.C. Xu, B.P. Xie, J.P. Hu, T. Zhang, and D.L. Feng, "Plain S-Wave Superconductivity in Single-Layer FeSe on $SrTiO_3$ Probed by Scanning Tunneling Microscopy", Nat. Phys. **11**, 946 (2015).

[21] L. Zhao, A. Liang, D. Yuan, Y. Hu, D. Liu, J. Huang, S. He, B. Shen, Y. Xu, X. Liu, L. Yu, G. Liu, H. Zhou, Y. Huang, X. Dong, F. Zhou, Z. Zhao, C. Chen, Z. Xu, X.J. Zhou, "Common Electronic Origin of Superconductivity in (Li,Fe)OHFeSe Bulk Superconductor and Single-Layer FeSe/$SrTiO_3$ Films", Nat. Commun. **7**, 10608 (2016).

[22] X.H. Niu, R. Peng, H.C. Xu, Y.J. Yan, J. Jiang, D.F. Xu, T.L. Yu, Q. Song, Z.C. Huang, Y.X. Wang, B.P. Xie, X.F. Lu, N.Z. Wang, X.H. Chen, Z. Sun, and D.L. Feng, "Surface Electronic Structure and Isotropic Superconducting Gap in $(Li_{0.8}Fe_{0.2})$OHFeSe", Phys. Rev. B **92**, 060504(R) (2015).

[23] Y.J. Yan, W.H. Zhang, M.Q. Ren, X. Liu, X.F. Lu, N. Z. Wang, X.H. Niu, Q. Fan, J. Miao, R.

Tao, B.P. Xie, X.H. Chen, T. Zhang, D.L. Feng, "Surface Electronic Structure and Evidence of Plain S-Wave Superconductivity in ($Li_{0.8}Fe_{0.2}$)OHFeSe", Phys. Rev. B **94**, 134502 (2016).

[24] B. Pan, Y. Shen, D. Hu, Y. Feng, J.T. Park, A.D. Christianson, Q. Wang, Y. Hao, H. Wo, Z. Yin, T.A. Maier and J. Zhao, "Structure of Spin Excitations in Heavily Electron-Doped $Li_{0.8}Fe_{0.2}$ODFeSe Superconductors", Nat. Commun. **8**,123 (2017).

[25] J.P. Rodriguez, "Spin Resonances in Iron-Selenide High-T_c Superconductors by Proximity to Hidden Spin Density Wave", Phys. Rev. B **102**, 024521 (2020).

[26] Pierre Ramond, *Field Theory. A Modern Primer* (Benkamin Cummings, Reading, 1981).